Physics of Fluids

RESEARCH ARTICLE | JANUARY 29 2024

Rheology of amino-functionalized graphene oxide suspensions in hydrogels FREE

Special Collection: Tanner: 90 Years of Rheology

Lorena R. da C. Moraes ; Hélio Ribeiro ; Ricardo J. E. Andrade ; Mônica F. Naccache

Check for updates

Physics of Fluids 36, 013122 (2024)
https://doi.org/10.1063/5.0185524

View Online
Export Citation
CrossMark

02 February 2024 10:55:50

AIP Publishing

Physics of Fluids ARTICLE pubs.aip.org/aip/pof

Rheology of amino-functionalized graphene oxide suspensions in hydrogels

Cite as: Phys. Fluids **36**, 013122 (2024); doi: 10.1063/5.0185524
Submitted: 31 October 2023 · Accepted: 30 December 2023 ·
Published Online: 29 January 2024

View Online Export Citation CrossMark

Lorena R. da C. Moraes,[1,a)] Hélio Ribeiro,[2] Ricardo J. E. Andrade,[2,3] and Mônica F. Naccache[1]

AFFILIATIONS

[1]Department of Mechanical Engineering, Pontifical Catholic University of Rio de Janeiro, Rio de Janeiro, Brazil
[2]Engineering School, Mackenzie Presbyterian University, São Paulo, Brazil
[3]MackGraphe, Mackenzie Institute for Research in Graphene and Nanotechnologies, São Paulo, Brazil

Note: This paper is part of the special topic, Tanner: 90 Years of Rheology.
[a)]**Author to whom correspondence should be addressed:** lorenarcmoraes@gmail.com

ABSTRACT

This work investigates the effects of amino-functionalized graphene oxide (AFGO) suspensions on the rheological behavior of Carbopol® hydrogels at pHs 5, 7, and 9. The AFGO concentration and media pH were evaluated and related to the suspension's microstructure and rheology. Graphene oxide (GO) nanosheets were synthesized using the modified Hummers method and functionalized with triethylenetetramine via microwave-assisted reaction to produce AFGO. The nanosheets were characterized by different techniques, such as scanning electron microscopy (SEM), thermogravimetric analysis, Raman spectroscopy, and x-ray photoelectron spectroscopy. The suspensions were characterized by rheological tests through steady-state and dynamic flow, zeta potential, and cryo-SEM for microstructure analysis. All samples presented a viscoplastic behavior and were modeled by the Herschel–Bulkley equation. Concerning the base hydrogels, the sample prepared at pH 9 showed lower viscosity, yield stress, and elastic modulus. At all pHs, the increase in the nanosheet concentration promotes a drop in the yield stress, viscosity, storage, and loss moduli. The cryomicrographs showed the impact of pH on the base hydrogel structure. It was also possible to observe that increasing nanoadditive concentration affects the Carbopol microgel swelling and weakens the suspension microstructure.

Published under an exclusive license by AIP Publishing. https://doi.org/10.1063/5.0185524

02 February 2024 10:55:50

I. INTRODUCTION

The graphene chemical functionalization, which consists of attaching functional groups on nanosheet surfaces and edges, has expanded its applications to commercial uses.[1,2] Functionalized graphene has greater chemical reactivity, and better dispersibility in different solvents and polymer matrices, besides being produced on a large scale.[3–5] Due to their characteristics, these nanosheets are truly relevant for developing fluids with superior properties.

The potential for applying functionalized graphene in complex fluids is enormous, as they are widely used in diverse areas. In addition to the properties expected through the suspension of functionalized graphene, the nanosheets can affect another determining feature for the fluid application: its rheological behavior.

Expressive results of functionalized graphene applications are presented for conductive 3D inks,[6–10] drilling fluids,[11–13] polymeric compounds,[14–19] lubricants,[20–25] medicinal gels and cosmetics,[26–28] filtration membranes,[29–31] cement pastes,[32–34] among others. However, information about the influence of graphene functionalization characteristics on the rheology of their suspensions in non-Newtonian dispersants is scarce. To the best of our knowledge, few reports still explore how the morphology of these nanosheets can affect the interactions that govern microstructures in complex dispersing media. On the other hand, knowing the rheology will allow understanding and optimizing the industrial processes including the flow of such nanofluids.

Among the few works that address the theme, Shang *et al.*[34] analyzed the interactions and rheology resulting from three types of suspensions in aqueous cement paste: a silica fume only, graphene oxide (GO) nanosheets with silica fume, and another silica fume encapsulated with GO (SFGO), suspensions. Taking the silica fume suspension as a reference, the rheological behavior of the GO nanosheets and silica fume suspension was different from the rheology presented by the SFGO suspension in the aqueous cement paste. While adding flat GO nanosheets caused a significant increase in viscosity, SFGO addition promoted the opposite. The authors related these results to the shape and surface activity of the GO and SFGO. Electrostatic interactions between the negative charges of the GO nanosheets and the cement particles can lead to flocculated structures that retain large amounts of water inside. This phenomenon increases the friction between the particles and consequently leads to the increase in the yield stress and in

Published under an exclusive license by AIP Publishing

the plastic viscosity and decreases the fluidity of the suspension. On the other hand, the SFGO has a spherical shape that adsorbs water molecules around its surface; this facilitates the roll of one particle on another and reduces the contact with the cement particles, reducing the friction resistance.[34] In addition, the negatively charged SFGO "spheres" provide repulsion between them, allowing better dispersion of cement particles and releasing the entrapped water. As a result, the increase in the SFGO concentration raised fluidity and reduced plastic viscosity.

Wang *et al.*[32] synthesized functionalized graphene oxide with polyether amine chains with different molar masses and evaluated its effects on the rheological behavior of cement paste. Differently from what happened for the GO suspensions, the addition of this modified graphene oxide (MGO) promoted an increase in the fluidity of the cement paste. Additionally, the higher the molar mass of the polyether amine chains, the better was the fluidity of the suspension. The authors suggest that the electrostatic repulsive force of MGO adsorption layers and polyether amine chain steric hindrance endowed a better cement paste fluidity.

From another perspective, Zhong *et al.*[10] reported the rheological effects of GO nanosheets on an aqueous geopolymer (aluminosilicate and alkaline-source particles) dispersion, aiming its application in 3D print. These authors demonstrated an increase in up to two orders of magnitude in the storage modulus of the GO suspension when compared to the geopolymer base fluid. Additionally, they indicated that the yield stress increases until a critical nanosheet concentration is reached; from then on, the increase in the GO portion causes a reduction in the yield stress, while the storage modulus continues to increase. The increase in the storage modulus was attributed to strong interactions between the GO nanostructure and the geopolymer. At the same time, the decrease in yield stress for higher GO concentrations was associated with lubrication effects between the nanosheets.

In our previous work,[35] the rheological effects of GO suspensions with different oxidation levels in Carbopol hydrogel [cross-linked poly (acrylic acid)] were investigated. The yield stress, viscosity, and elastic modulus decreased with increasing GO concentration. Furthermore, the nanosheets with a lower oxidation level favored a more accentuated drop in such rheological parameters. It was verified that the introduction of GO into the hydrogel weakened the microstructure of the system. In addition to the hydration and consequent swelling of the polymer chains, the rheological characteristics of the Carbopol hydrogel come from the high repulsion level between the macromolecules (at neutral pH). The GO–GO and GO–Carbopol repulsion levels are weaker than the Carbopol–Carbopol, which facilitates chains' mobility in the system.

Amino-functionalized graphene oxide (AFGO) is widely applied as an additive in the development of composites, membranes, and polymeric solutions.[29,36–39] It also stands out for having antimicrobial properties, presenting better performance than GO in some cases, showing great potential for biomedical uses, even in very low nanosheet concentrations.[40,41] AFGO can be synthesized through the amidation reaction of graphene oxide (GO), without causing much damage to the graphene structure.[40] One of the proposals for the insertion of amino groups on the GO is to increase the local density of positive charges on the nanosheets.[40] Continuing the previous work,[35] the intention is to analyze the influence of nanosheets containing positive charges on the suspension rheological behavior.

On the other hand, the Carbopol aqueous dispersion produces a yield stress fluid widely used in several industries and as a model fluid among rheologists[42] due to its non-toxicity, transparency, and ease of handling characteristics. The knowledge already established regarding the mechanisms that govern the complex character of the aqueous dispersion of Carbopol and the simplicity of such hydrogel composition makes it an ideal base fluid for conducting fundamental studies.

The AFGO characteristics, especially the antimicrobial ones, and the extensive use of Carbopol made the combination of these materials highly attractive to develop new materials, mainly in the biomedical, pharmaceutical, and cosmetic industries. The study of this system can be of great relevance for preparing new creams, ointments, and gels, for example.

Additionally, fundamental studies about the internal microstructure and mechanisms that govern the rheology of AFGO suspensions on Carbopol hydrogel may serve as a starting point to propose combinations of materials. Some examples are nanomaterials containing different configurations/morphologies with other kinds of polyelectrolytes or polymer configurations, intending to develop several products or manufacturing protocols.[6–9,43] In this way, this kind of study becomes strategic so that nanofluids can be increasingly used in industrial processes and, finally, by society.

In this context, this study aims to contribute to analyzing the effects of graphene derivative suspensions in the rheology of yield stress fluids. This work investigated the rheological effects of amino-functionalized graphene oxide suspensions in Carbopol® hydrogels. The effects of the hydrogel pH and the AFGO concentration were also evaluated.

II. MATERIALS AND EXPERIMENTAL METHODS

A. Synthesis of graphene oxide (GO) and amino-functionalized graphene oxide (AFGO)

In general, graphite oxidation was performed through the modified Hummers method.[44] Then, based on the microwave-assisted reaction, the amine-functionalization route followed the work of Ribeiro *et al.*[45] A mixture of triethylenetetramine (TETA) and GO was placed in a microwave reactor. After the reaction finalization and the system's cooling, the mixture was filtered and washed carefully with anhydrous ethanol to remove the excess TETA that did not react. The filtered material was dried, and the exfoliation of AFGO was performed as a step in the nanofluid preparation. Details about the complete methodology used for the GO and AFGO production can be seen in Sec. S1 of the supplementary material.

B. Preparation of pure Carbopol hydrogel and amino-functionalized graphene oxide (AFGO)/Carbopol suspensions

To prepare hydrogel, Carbopol® Ultrez 10 from Lubrizol Corporation was utilized. Carbopol® is a polyacrylic acid of high molecular weight with cross-linking points.[46–48] A fixed Carbopol concentration of 0.3 wt. % was used for all prepared samples.

In order to investigate the influence of nanosheet ionization on system rheology, suspensions were prepared at pHs 5, 7, and 9. The relative amount of sodium hydroxide (NaOH) added to the system is the determining factor for obtaining the intended pH. Suspensions with 1 and 5 mg/mL of the AFGO concentration were prepared. For comparison purposes, pure Carbopol hydrogels were prepared for all investigated pHs.

02 February 2024 10:55:50

Published under an exclusive license by AIP Publishing

Further details on preparing the Carbopol base fluids and the AFGO suspensions in the hydrogels are available in Sec. S2 of the supplementary material.

C. Characterization of GO and AFGO nanosheets

The physicochemical characterization of GO and AFGO is an important step to evaluate the morphology, chemical composition, and structure of the nanosheets produced, as well as to determine whether the modification process used was successful. Raman spectroscopy, thermogravimetric analysis (TGA), and X-ray photoelectron spectroscopy (XPS) tests were carried out. Further details about the methodology and characterizations used are available in Sec. S3 in the supplementary material.

D. Characterization of the suspensions

1. Rheological measurements

Rheological experiments were carried out using the stress controlled rotational rheometers AR-G2 and DHR-3, both from TA Instruments. The geometries employed were the cross-hatched parallel plates (with a gap of 1 mm and a diameter of 60 mm), and in some cases, the grooved concentric cylinders (with a cup diameter of 30 mm, a bob diameter of 28 mm, and an operating gap of 4 mm). All tests were performed at standard room temperature (25 °C) and under atmospheric pressure. Additionally, all tests were carried out in triplicate.

The rheology of suspensions was investigated for steady-state and oscillatory flow tests. Flow curves with shear rates ranging from 1000 to 0.01 s^{-1} were obtained. For every test, the samples rested for 10 min in order to reach thermal equilibrium and allowing the fluid microstructure to recover after loading. Additionally, parameters aiming to guarantee the attaining of a steady state were applied to record each point. Every 10 s, the average torque was measured, and after three successive 10 s intervals, the average torques are compared. A steady state is presumed to exist when the differences are less than 0.1% or for a maximum of 1200 s. As the base fluid is non-Newtonian, the Weissenberg–Rabinowitch equation was used to perform the stress correction through a TA Instruments software. For oscillatory flow tests, stress and frequency sweep experiments were conducted. For stress sweep, measurements of the storage (G') and loss (G'') moduli were performed concerning a stress amplitude ranging from 0.1 to 100 Pa, with a frequency of 1 Hz. In measures of frequency sweep, G' and G'' curves vs frequency amplitude, with a stress amplitude of 0.1 Pa, were registered. Hysteresis tests were performed to assess the effects of time. In this experiment, two flow curves were measured in succession. The shear rate was increased from 0.01 to 1000 s^{-1} for the first flow curve and then decreased from 1000 to 0.01 s^{-1} for the second flow curve. The comparison between the curves was analyzed.

2. Zeta potential

Zeta potential measurements were performed to analyze the stability of the suspensions. The equipment used was a Zetasizer, model Nano ZS90, by Malvern Panalytical, with 632.8 nm laser and polycarbonate DTS1070 zeta cell with gold-plated electrodes.

Samples of pure Carbopol hydrogels, pure aqueous AFGO dispersions, and 1 mg/mL of AFGO suspensions in the hydrogel, for all pHs (5, 7, 9), were dispersed in aqueous solutions with their respective pH, in the proportion of 1:10 to perform the measurements.

3. Cryo-SEM

The microstructures of the base fluids and suspensions were visually examined using cryo-SEM, employing the TESCAN-CLARA field-free Ultra High Resolution (UHR) scanning electron microscope with a Quorum PP3000T cryogenic system. The samples were frozen by diving them quickly in liquid nitrogen for 30 s at −210 °C under vacuum (to avoid the formation of ice crystals in the water). Then, they were placed in a preparation chamber at −170 °C and subjected to a sublimation process (at −60 °C for 15 min) to remove water; after that, they were coated with a thin platinum layer at 10 mA for 120 s. The samples were also inserted into the microscope chamber, which was maintained under a high vacuum at −140 °C. The micrographs were taken at 5 kV.

III. RESULTS AND DISCUSSION

A. Physical–chemical aspects of graphene oxide (GO) and amino-functionalized graphene oxide (AFGO) nanosheets

In general, the SEM images of GO and AFGO (Fig. S1 in supplementary material) showed nanosheets with lateral sizes larger than 2 μm, containing irregular textures and rough ripples, which are characteristic of graphene.[35] Raman spectrum of GO and AFGO nanosheets showed the presence of the main characteristic bands of graphene: D, G, and 2D, presenting different structural aspects after the functionalization process, as expected. TGA showed that AFGO nanosheets present a loss of mass around 9% between 212 °C and 350 °C, associated with TETA degradation; such behavior was not found for the GO sample. AFGO XPS showed the presence of C1s, O1s, and N1s photoemissions peaks, which are associated with carbon, oxygen, and nitrogen bonds, indicating the introduction of TETA covalently to the AFGO nanosheets.

Therefore, the chemical characterization of AFGO showed that aminated groups were introduced to the nanomaterial. The complete discussion of SEM, Raman, TGA, and XPS results is present in Sec. S4 in the supplementary material.

B. Rheological and structural aspects of the suspensions

In advance, it is worth emphasizing that the pH variation of the suspensions will influence both the ionization of the Carbopol chains and the AFGO nanosheets. The increase in pH generally promotes higher deprotonation of the carboxylic acid groups on the polymer and GO nanosheets. In contrast, when the pH decreases, the amine groups present on the AFGO surface behave like a Lewis base, receiving H^+ protons, hence giving to the nanosheets a partially positive charge due to the formation of the $-NH_3^+$ species.

Thus, it is essential initially to observe and discuss the influence of pH on the properties of the base fluid, i.e., the Carbopol hydrogel. The ionization level of this carbomer determines its intra and intermolecular interactions, which will influence the rheological behavior. Figures 1(a) and 1(b) display the flow curves and the stress sweep of the Carbopol hydrogels at pH 5, 7, and 9.

02 February 2024 10:55:50

Published under an exclusive license by AIP Publishing

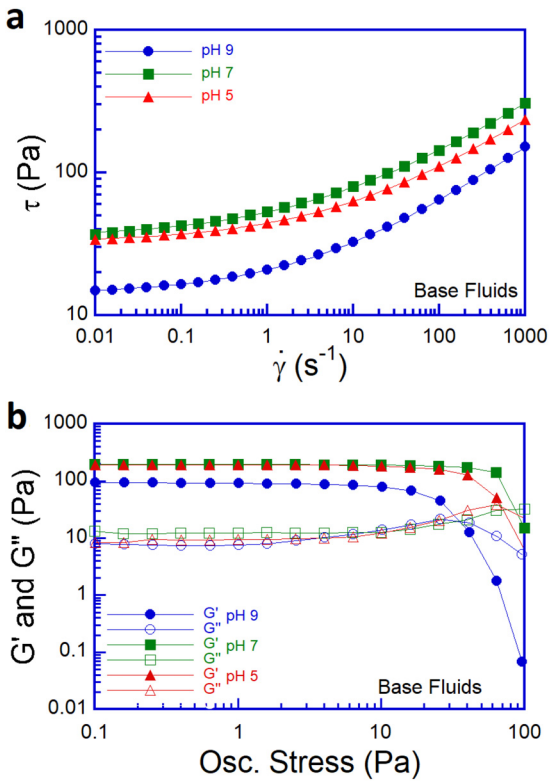

FIG. 1. Carbopol hydrogel rheology at different pHs. (a) Flow curves of base fluids obtained experimentally (symbols) and Herschel–Bulkley curve fitting (continuous lines). (b) Stress sweep curves (filled symbols indicate G′ and empty symbols represent G″). From the Herschel–Bulkley fitting, the following parameters were obtained: pH 5: τ_y (Pa) = 32.3, k (Pa s^{-n}) = 11.8, n = 0.41; pH 7: τ_y (Pa) = 33.9, k (Pa s^{-n}) = 18.1, n = 0.39; pH 9: τ_y (Pa) = 14.4, k (Pa s^{-n}) = 7.1, n = 0.43.

At the appropriate pH, pure Carbopol aqueous dispersion is a model yield stress fluid that usually fits the Herschel–Bulkley model,[49–51] given by Eq. (1)—where η represents the apparent viscosity, k is the consistency index, $\dot{\gamma}$ is the shear rate, n is the flow index, τ_y is the yield stress, and τ is the shear stress,

$$\eta = \begin{cases} (k\dot{\gamma}^{\,n-1} + \tau_y/\dot{\gamma}), & \tau \geq \tau_y, \\ \infty\,(\dot{\gamma} = 0), & \tau < \tau_y. \end{cases} \tag{1}$$

This behavior is commonly observed in dispersions above a critical polymer concentration. Such fluids maintain an irregular internal order, forming three-dimensional structures with sufficient rigidity to withstand external stress, as long as it is lower than the yield stress, offering flow resistance.[49] At the yield stress, the structure breaks, leading to a steep decrease in the viscosity, followed by a shear thinning behavior as the applied stress increases.

Figure 1(a) illustrates the flow curves of pure Carbopol hydrogels at pH 5, 7, and 9. Upon examining the flow curves, the asymptotic trend of the stress curves under low shear rates indicates the presence of yield stress; conversely, an increase in shear rate results in a non-linear escalation in shear stress. This behavior is described by the Herschel–Bulkley equation.

In Fig. 1(a), the flow curves are fitted using the Herschel–Bulkley model, and their parameters are given in the subtitle. It can be observed that the flow index is below 1, indicating that these hydrogels exhibit shear thinning behavior at higher shear rates.

The pH 7 sample shows the highest stress values for the applied shear rate range, closely followed by the pH 5 gel. This result was expected since the Carbopol supplier indicates in its datasheet a range of pH where a kind of viscosity "plateau" occurs for samples submitted to the same shear rate.[52] The pH 9 hydrogel comes in third, with lower stress values than the gels with pH 7 and 5.

Figure 1(b) shows the behavior of the storage (G′) and loss moduli (G″) of the hydrogels subjected to a stress sweep range. In general, as with the flow curves, the samples showed similarities. It is possible to distinguish three characteristic regions of Carbopol aqueous dispersion. The first region is identified as the linear viscoelastic region (LVR). It refers to the portion of the curve in which G′ and G″ are constant, or, in other words, they are independent of the applied stress amplitude.[50,53–57] The stress applied in such a region does not have the necessary intensity to break the interactions that maintain the fluid microstructure.[57] For all analyzed samples, G′ is larger than G″ in the LVR, indicating that in lower stress amplitudes, such microstructure promotes the predominance of elastic behavior and low internal dissipation. Then, the molecules that form the system can deform elastically but do not move significantly from their original positions.

The successive increase in the stress amplitude drives the appearance of a transition region. This second region is located at intermediate stress amplitudes, starting where the moduli are no longer constants and ending where the crossover between G′ and G″ occurs. While G′ starts to decrease, G″ starts to increase, which indicates the beginning of the drop in elasticity and the breakdown of the initial microstructure.[55] Within this region, parts of the fluid microstructure start to fail, i.e., molecules shift extensively from their initial locations. The increase in G″ is caused by the dissipation of mechanical energy produced by molecular motion. Nonetheless, the fluid microstructure is still strong enough to sustain a significant elastic response; hence, G′ remains large.[50]

The more significant increase in the stress amplitude creates a third region, which is also a non-linear zone and begins after the crossover point between G′ and G″. The storage modulus rapidly declines to values smaller than G″. On the other hand, the loss modulus grows until it reaches a maximum value and then decreases in sequence. Such stress magnitudes produce significant microstructure breakdowns in the fluid, causing it to display viscous behavior. As the applied stress amplitude increases, the fluid structuring level reduces, and the elastic response also decreases.[50]

Such G′ and G″ curve profiles also indicate that the samples have yield stress. Among other methods, some authors consider the stress amplitude where the crossover point (or characteristic modulus) occurs as a measure of yield stress.[58–60] Quantitatively, the yield stress obtained from the characteristic modulus may differ somewhat from the shear yield stress measured in the steady-state mode.[61,62]

When comparing the hydrogels with different pH, the curves of G′, G″, and the crossover point (where G′ = G″) show similar response patterns to those observed for the flow curves. In descending order: the hydrogel prepared with pH 7 presents the highest values for both modules and crossover point, followed by the curves of the gel with pH 5, which exhibit lower values of G′, G″, and crossover point but are very

02 February 2024 10:55:50

Published under an exclusive license by AIP Publishing

close to those verified for the hydrogel with pH 7; finally, the Carbopol base fluid with pH 9 presented the smallest moduli and crossover point. The same behavior is observed for the yield stress and apparent viscosity.

The observed effects of pH variation on the rheological behavior of Carbopol hydrogels can be justified by the polymer chain intra and intermolecular interactions under the addressed conditions. Beforehand, it is crucial to know the structure and composition of the Carbopol chain. This carbomer contains groups of carboxylic acids distributed throughout the polymer backbone, with cross-linking points joining various parts of its chain. Since carboxylic acids are weak acids, depending on the medium pH, they can lose H^+; in other words, they can deprotonate.[51,53–55,63–66]

The Carbopol hydrogel with pH 7 has a strongly ionized polymer chain since the medium pH is higher than the polymer pKa. According to the manufacturer, the carboxylic acids of Carbopol (for grade Ultrez 10—Lubrizol) have pKa of 6.0 ± 0.5.[67] In parallel, in this system, the concentration of ions within the microgels is higher than in the surroundings, promoting a significant osmosis process in the macromolecule due to the Donnan equilibrium.[68–70] Therefore, there is considerable swelling of the microgel. As a result, the 0.3% wt. of polymer concentration and the high volume of the microgels in the network provide a hydrogel with a consistent structure, presenting the highest values of yield stress, apparent viscosity, and storage and flow moduli.

The Carbopol hydrogel with pH 5 has a lower degree of ionization than the base fluid with pH 7, having fewer ions in the microgels. Conversely, for pH 5, the concentration of ions in the solvent is also reduced, so significant osmosis must occur. Nonetheless, another relevant concept can be related to the proximity of the rheological behaviors found in these hydrogels. An elasticity effect, associated with the number of cross-linking points in the polymer, limits the volumetric expansion of the Carbopol macromolecule.[68] This means that even if the ionization degree increases, the microgel volume will not grow anymore.[71] As the pH 5 of the medium is close to the pKa of Carbopol, the ionization of the chain is considerable, and the microgel may be closer to its swelling limit. In contrast, the microgels subjected to the medium with pH 7 may have already reached such a limit.

Adding more NaOH to prepare the hydrogel at pH 9 strongly influenced the swelling of the Carbopol macromolecules. It occurs because, as the amount of NaOH increases, the amount of ions in the system also increases, especially Na^+ cations. From an electrostatic point of view, a high density of counterions in the dispersion reduces the level of repulsion of the anions on the polymer chain. As a result, both the polymer swelling and the repulsion between adjacent microgels are reduced. The internal osmotic pressure of Carbopol microgels at pH 9 is significantly reduced compared to hydrogels prepared at lower pH. The higher amount of ions in the solution decreases the difference in the concentration of ions inside and outside the microgel. Consequently, there is less solvent retention in the macromolecule, inhibiting the polymer's swelling capability. The association of these events leads to the formation of a gel with a more fragile structure.

The effects of AFGO suspensions on the flow curves of the hydrogels are shown in Fig. 2. As obtained for the base fluids, all suspensions follow the Herschel–Bulkley model, presenting yield stress and nonlinear growth of shear stress with increasing shear rate. Table I shows the values of the Herschel–Bukley model parameters for the samples and also indicates the pseudoplastic behavior of the systems.

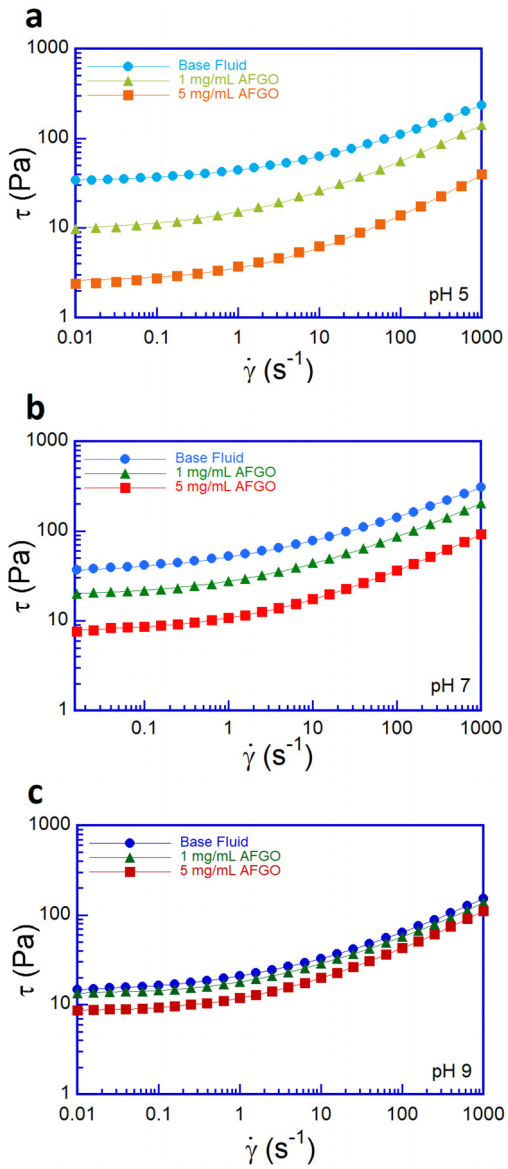

FIG. 2. Effects of AFGO suspensions on the flow curves of the hydrogels. (a) Flow curves of the samples at pH 5. (b) Flow curves of the hydrogels at pH 7. (c) Flow curves of the suspensions at pH 9. The curves formed by symbols reflect the experimental results, while the curves formed by solid lines correspond to the Herschel–Bulkley curve fittings.

Figure 3 presents the results of stress sweep oscillatory tests of the AFGO suspensions. All samples presented a storage modulus higher than the viscous modulus in the LVR, with a crossover point occurring for larger stress amplitudes.

Upon joint analysis of the data presented in Table I and the curves illustrated in Figs. 2 and 3, it becomes evident that for all investigated pH values, the addition and rise in the concentration of the AFGO in the hydrogels promote a drop in the storage and loss moduli, in the yield stress, and in the apparent viscosity (since there is a

02 February 2024 10:55:50

Published under an exclusive license by AIP Publishing

TABLE I. Effects of AFGO concentration on the Herschel–Bulkley fitting parameters of the hydrogel suspensions at different pHs. Where ϕ is the AFGO concentration in mg/mL, τ_y is the yield stress in Pa, k is the consistency index in Pa s^{-n}, and n is the flow index (dimensionless).

Parameters	pH 5			pH 7			pH 9		
ϕ	0	1	5	0	1	5	0	1	5
τ_y	32.3	10.9	2.5	33.9	18.4	7.5	14.4	12.8	8.4
k	11.8	5.7	0.9	18.1	9.3	3.4	7.1	5.6	3.9
n	0.41	0.47	0.53	0.39	0.44	0.47	0.43	0.43	0.47

downfall of the stress curves compared with the base fluids). Another characteristic is the increase in the flow index (n) with increasing nanosheet concentration, indicating a reduction in the pseudoplastic character of the suspensions.

The samples prepared at pH 5 displayed more pronounced declines in rheological parameters induced by AFGO suspensions; their curves are in Figs. 2(a) and 3(a). Comparing the values in Table I, the suspension with 1 mg/mL of AFGO at pH 5 shows a drop of 66% in the τ_y in relation to the base fluid, while the 5 mg/mL suspension shows a drop of 92%.

In parallel, there is a larger increase in n with increasing AFGO concentration in these samples. The storage modulus of the 5 mg/mL AFGO suspension is approximately ten times smaller than the G′ of the base hydrogel; the same occurs for the loss modulus. Furthermore, the LVR of the suspension with a higher concentration of nanosheets occurs only at lower stress amplitudes, with the crossover point occurring for stress amplitude almost two orders smaller than that found for the pure hydrogel.

Figures 2(b) and 3(b) display the suspensions' flow curves and stress sweep tests at pH 7. AFGO suspensions in the hydrogel at pH 7 also yielded a significant decrease in shear stress values, G′, and G″, albeit to a lesser extent than observed for the pH 5 suspensions. The yield stress values were reduced by 46% for the 1 mg/mL suspension and 78% for the 5 mg/mL suspension. Furthermore, the suspensions at pH7 hydrogel showed reduced LVR, undergoing irreversible deformations at lower stress amplitudes. The crossover point of the 5 mg/mL suspension is approximately one order of magnitude lower than that found for the pure hydrogel.

Conversely, the suspensions prepared at pH 9 showed the slightest variation of the rheological behavior with increasing AFGO concentration. Figure 2(c) presents the flow curves, while Fig. 3(c) displays the stress sweep curves of the AFGO suspensions in pH 9 hydrogel. The reduction in the storage and loss moduli, in the crossover point stress amplitude, and the shortening of LVR still occur, but they were significantly less pronounced. The closeness of the flow curves for pH 9 suspensions compared to the samples prepared at lower pH levels is evident. Examining the Herschel–Bulkley parameters, the pH 9 hydrogel dropped 11% and 42% in the yield stress of suspensions containing 1 and 5 mg/mL, respectively. These results indicate that the pH medium also influences the effects of the AFGO suspension over hydrogel rheology.

The mechanical response of the material microstructure in its quiescent condition can be evaluated using frequency sweep tests. During the test, a constant stress is maintained low enough to ensure the experiment is conducted in the linear viscoelastic regime

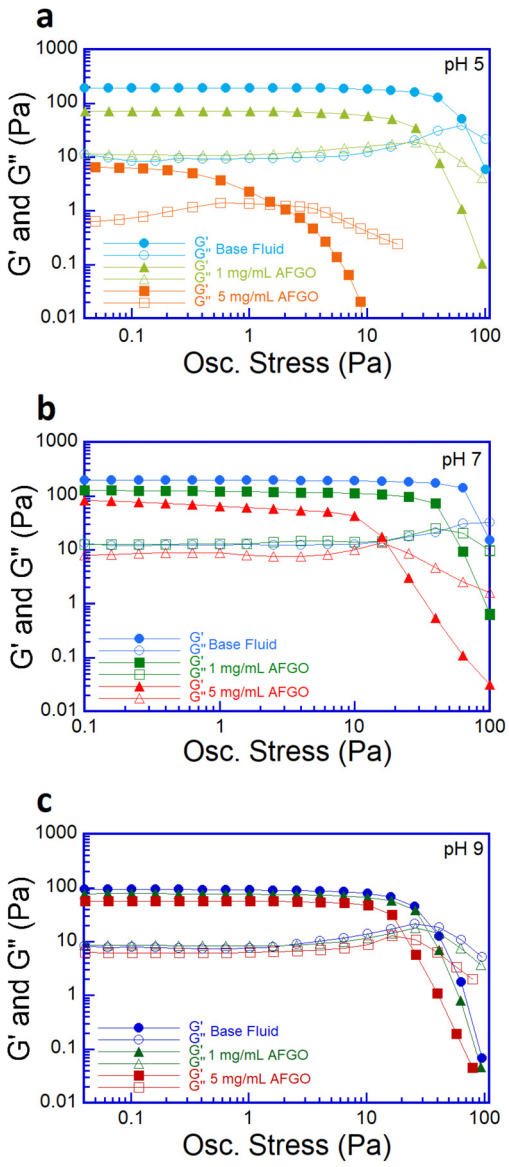

FIG. 3. Effects of the AFGO concentration on the stress sweep curves of the hydrogels. (a) Stress sweep curves of the samples at pH 5. (b) Stress sweep curves of the hydrogels at pH 7. (c) Stress sweep curves of the suspensions at pH 9. Filled symbols correspond to G′ and empty symbols represent G″.

throughout the frequency range. Figures 4(a)–4(c) show the effects of the AFGO concentration on suspensions with pH 5, pH 7, and pH 9, respectively, subjected to frequency sweep. Due to technical–experimental issues, the results are presented for a reduced range of frequency oscillation.

Frequency sweep oscillatory tests show the same trend observed in previously presented experiments. All samples show G′ constant and larger than G″, i.e., the data are within the rubbery region, generally observed for viscoelastic solids and reticulated systems.[50,72] The G″ curves, on the other hand, increase with frequency, indicating that

02 February 2024 10:55:50

Published under an exclusive license by AIP Publishing

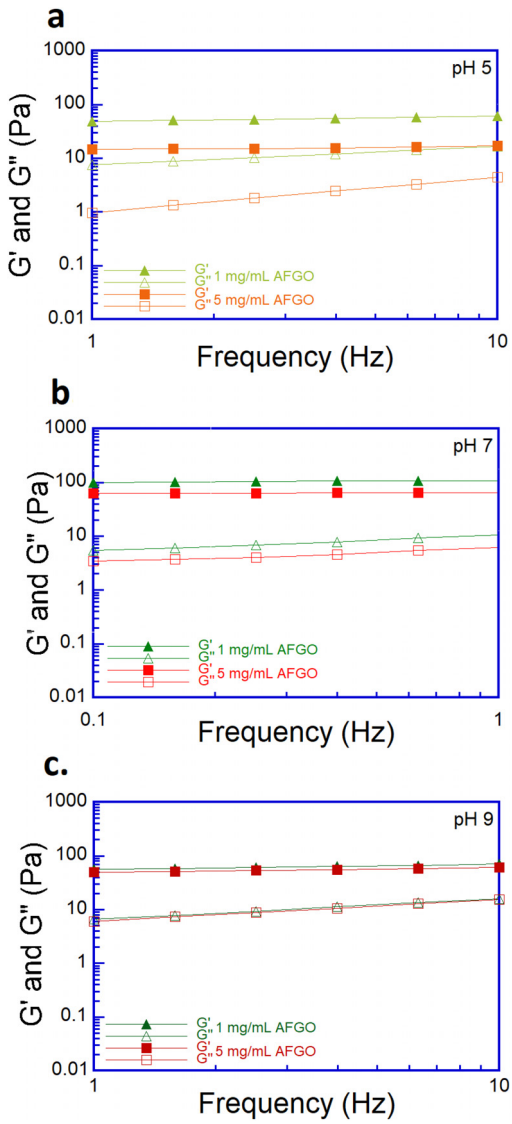

FIG. 4. Effects of the AFGO concentration on the frequency sweep curves of the hydrogels. (a) Frequency sweep curves of the samples at pH 5. (b) Frequency sweep curves of the hydrogels at pH 7. (c) Frequency sweep curves of the suspensions at pH 9. Filled symbols correspond to G′ and empty symbols represent G″.

more mechanical energy is dissipated at larger frequencies.[50] Once more, AFGO displays a larger effect on suspensions made at pH 5, as seen by a more noticeable decrease in storage and loss moduli as the nanosheet concentration rises. After that, suspensions prepared at pH 7 exhibit an intermediate decrease in modulus values. Ultimately, pH 9 suspensions have a minor drop in storage moduli, while viscous moduli remain similar.

Figures 5(a) and 5(b) show the relative behavior of the yield stress and the storage modulus (obtained from the stress amplitude sweep test in LVR) concerning the pH and AFGO concentration of the suspensions. In order to observe the trend of rheological behavior, disregarding the absolute values of the parameters, τ_y and G′ were

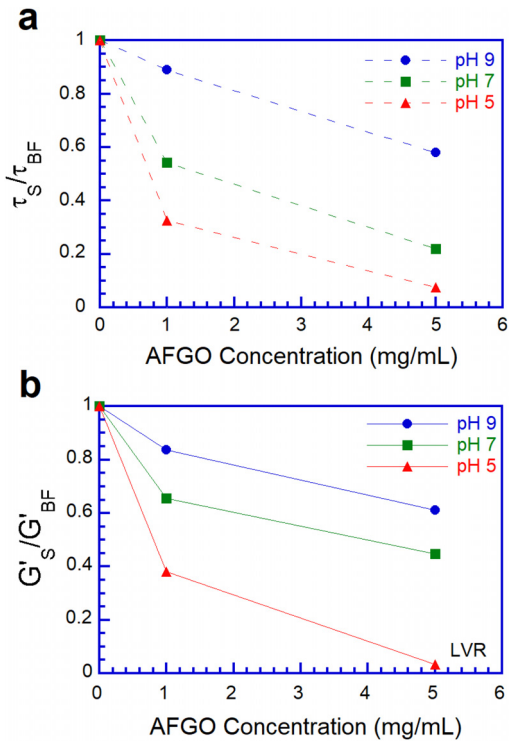

FIG. 5. Overview analysis of the pH and AFGO concentration effects on some rheological parameters of the suspensions. (a) Normalized yield stress. (b) Normalized storage modulus.

normalized, i.e., the parameter values found for each sample (τ_{yS} and G'_S) were divided by the respective values obtained for the base fluid (τ_{yBF} and G'_{BF}).

Upon analyzing the graphs presented in Fig. 5, it is evident that the addition of nanosheets significantly impacts the rheological parameters of hydrogels, even at lower concentrations. Additionally, it becomes even more notorious that raising the AFGO concentration in the hydrogels exerts a more intense effect on suspensions at lower pH values.

Thixotropy and viscoelasticity express time and shear history effects. Both behaviors exhibit common phenomena such as shear thinning, hysteresis, and stress overshoots during startup experiments.[73] Although no time-dependent fluids may display hysteresis, the emergence of dynamic hysteresis in rheological data are often regarded as a sign of thixotropy.[74] Hysteresis tests were conducted to verify the possibility of the suspensions presenting thixotropy. Figures 6(a)–6(c) present the results of the ascending and descending flow curves for suspensions with pH 5, pH 7, and pH 9, respectively.

First, it is worth mentioning that the curves presented in Fig. 6(a), for suspensions with pH 5, were obtained after applying a preshear of $500\,s^{-1}$ for 2 min and with an equilibrium time of 5 min. Applying pre-shear was necessary because the ascending shear rate curves, especially for higher concentrations, did not present repeatability in the results, unlike the descending curves. After applying preshear, the ascending and descending curves were coincident for both suspensions, with 1 and 5 mg/mL of AFGO. It is an indication that

02 February 2024 10:55:50

Published under an exclusive license by AIP Publishing

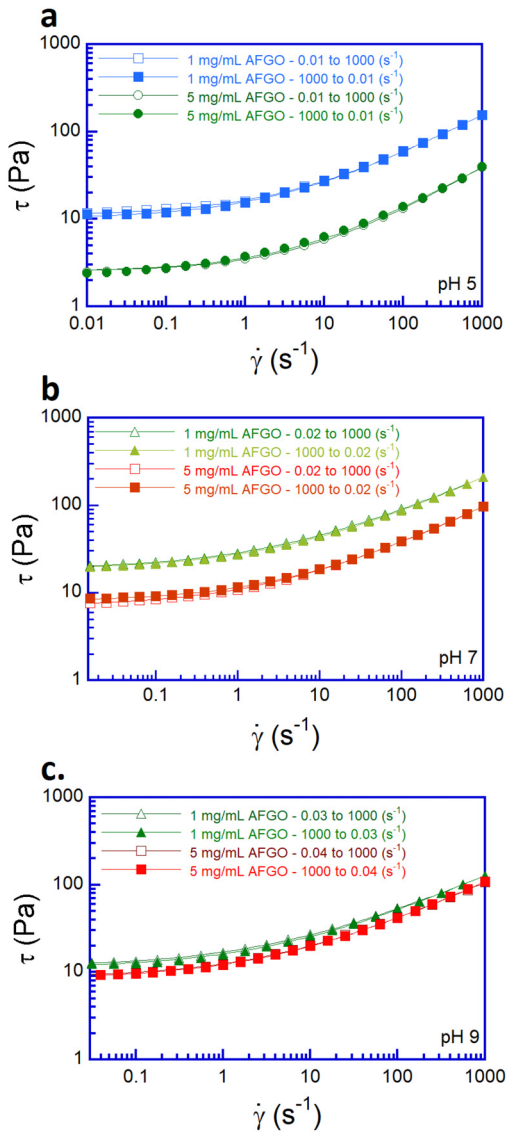

FIG. 6. Hysteresis tests performed with (a) pH 5 suspensions; (b) pH 7 hydrogels; and (c) pH 9 samples. Empty symbols indicate an upward shear rate, while filled symbols indicate a downward shear rate.

suspensions at pH 5 did not present thixotropy. However, the need to pre-shear these samples indicates that the shear history influences suspensions at pH 5.

The suspensions prepared at pH 7 and pH 9 did not require pre-shear. Such samples showed repeatability in all measured curves. Furthermore, the upward and the downward shear rate curves showed similar results in each suspension analyzed, indicating that the presence of nanosheets did not develop any relationship or interaction that would lead the rheological characteristics of the hydrogels to be time-dependent, or in other words, it did not promote thixotropy.

Zeta potential analyses were conducted with Carbopol dispersion, AFGO suspension, and the suspension of the two materials (Carbopol-AFGO) in aqueous solutions, adjusted to pHs 5, 7, and 9. The results are displayed in Table II. It is worth mentioning that factors such as concentration, size and shape of particles, solvents, pH, and temperature, among others, influence electrophoretic mobility and, therefore, the zeta potential.[75] As previously discussed, the mechanisms affecting the hydrogels' rheology at the analyzed pHs differ. Therefore, it would not be sensible to compare and associate the magnitude of Carbopols' zeta potential under different pH with the base hydrogels' rheological behaviors, since factors such as microgel volume are also modified in addition to the surface charge. In this sense, the main aim is to evaluate the variation in the zeta potential of materials subjected to the same pH.

TABLE II. Effects of pH 5, pH 7, and pH 9 on zeta potential of Carbopol macromolecules, AFGO nanosheets, and the system containing both materials.

	ζ (mV)		
pH	Carbopol	AFGO	Carbopol-AFGO
5	−65.7	−37.4	−44.5
7	−102.0	−41.1	−79.5
9	−77.0	−43.9	−73.2

Upon examining Table II, the initial finding is that the zeta potential shows negative values in all measurements, even the AFGO at pH 5, which is expected to have a larger degree of amino group acting as a Lewis base. This suggests that not enough amino groups were added to the nanosheets during synthesis to cause the net surface charge of AFGO to become fully positive, which is consistent with the TGA results. The higher concentration of oxygenated groups maintains the net surface charge negative even when the positively charged groups are present on the nanosheets. Additionally, all systems have a zeta potential below −30 mV, indicative of the colloidal stability of macromolecules and nanosheets.

For all pHs analyzed, Carbopol has the highest zeta potential module value regarding the other systems, indicating a material that contains a surface highly charged with negative ions, which is a determining factor for the formation of the "jammed structure" that promotes the rheological characteristics of the gel.[51,53–55,63–66] In the case of base hydrogel at pH 5, less than half of the carboxylic acids in Carbopol are deprotonated, which is why the zeta potential module value is lower when compared to the dispersion at pH 7. On the other hand, another phenomenon can be connected to the lower zeta potential module of Carbopol dispersed in a pH 9 medium. With the higher concentration of counterions in the solvent, there is a partial neutralization of the anions on the macromolecule due to the counterion condensation.

Regarding the AFGO nanosheets, the results indicate that the increase in pH promotes an increase in the module value of the zeta potential. The increase in pH promotes the deprotonation of carboxylic acids due to the increased hydroxyl anion concentration in the solvent. Concerning the nitrogen groups in the AFGO nanosheets, the lower the pH media, the higher their Lewis basic character. This behavior also contributes to a lower zeta potential module value for lower pHs. In other words, in addition to lower deprotonation of oxygen, higher is the basic character of nitrogen groups, leading to a reduction in the module value of the zeta potential for lower pH.

02 February 2024 10:55:50

Published under an exclusive license by AIP Publishing

The zeta potential results for the AFGO-Carbopol system showed intermediate module values—lower than those found for the pure Carbopol hydrogels and higher than the ones registered for the AFGO nanosheets at their corresponding pHs. Such behavior is consistent with the drop in viscosity, yield stress, and elasticity of the suspensions concerning the base fluids. Being formed by a jammed structure, the level of repulsion between the microgels present in the system is decisive for forming the rheological profile of the Carbopol hydrogel. The AFGO nanosheet suspension in the Carbopol gel facilitates the movement of the polymer chains under shear as the Carbopol–Carbopol repulsion is higher than the AFGO-Carbopol repulsion. This could be one of the factors that affect the rheological behavior of the suspension with increasing concentration of the nanosheets.

Interestingly, the drop in the zeta potential module value for the Carbopol-AFGO system is proportionally superior for the medium with pH 5. Concerning the Carbopol dispersion with the respective pH, the zeta potential module of the Carbopol-AFGO system for pH 5 showed a drop of 32%, while for pH 7, the decrease was 22%, and for pH 9, it showed a drop of just 5%. Such results are in line with the trend observed in the rheological data. Furthermore, this indicates that factors other than just the lower level of repulsion between AFGO and Carbopol contribute to the rheological effects of AFGO suspension in the hydrogels.

The AFGO suspension in the hydrogel may affect the deprotonation and swelling of Carbopol macromolecules. Introducing AFGO to the hydrogel also increases the concentration of –COOH groups in the medium. The acids in the system will influence the balance of H^+ concentration; however, the pKa of carboxylic acids in AFGO is around 4.2, smaller than the Carbopol one. Therefore, AFGO acids will present a higher ionization degree. In order to maintain an ionic balance, Carbopol deprotonation is reduced at low pH values. It is even possible that the Carbopol pKa is being modified (increasing).[76,77] Therefore, the polymer's net surface charges decrease, which leads to a reduction in intra and intermolecular repulsion. As a result, the microgel swelling and its interaction with the surrounding particles are reduced.

AFGO suspension may also be affecting microgel osmosis (the Donnan equilibrium). With the deprotonation of AFGO, the system begins to have a higher amount of ions in the surrounding solvent and a lower concentration of ions within the microgel concerning the dispersion of pure Carbopol, resulting in a reduction in microgel osmosis. Due to the combination of these factors, the macromolecule experiences reduced swelling. Consequently, as the concentration of nanosheets in the system increases, the rheological parameters of the suspensions, such as viscosity, yield stress, and elastic and viscous moduli, decrease.

As seen, suspensions at pH 5 are the most affected rheologically. This may be occurring because, in addition to presenting the lowest level of Carbopol-AFGO repulsion, as they are at a pH below of the Carbopol pKa, the suspensions prepared at pH 5 are those that present the most pronounced impact of the nanosheets on the macromolecule swelling, resulting in a significant reduction of the volume and surface charge of microgels. This further decrease in Carbopol ionization can be observed through the heightened decrease in the zeta potential magnitude found in the AFGO-Carbopol system compared to the Carbopol dispersion. Such mechanisms promote the formation of a more fragile hydrogel.

Suspensions with pH 7 are also significantly affected; however, as the pKa of Carbopol is lower than the pH of the medium, the impact of the AFGO suspension on the deprotonation and osmosis of the macromolecule is smaller, leading to lower levels of reduction in the microgel volume compared to suspensions prepared at pH 5. pH 9 is well above the pKa of both the acidic groups of Carbopol and AFGO nanosheets. Therefore, the addition of nanosheets to the system does not influence the deprotonation of the polymer. On the other hand, the high concentration of counterions in the solvent is the main factor impacting the microgel's osmosis and intermolecular repulsion level. Thus, the aspect that has the greatest effect on reducing the rheological curves of suspensions at pH 9 is the interaction strength between Carbopol and AFGO, which is smaller than the Carbopol–Carbopol interaction.

Visual microstructure analysis of the base hydrogels and suspensions further contributes to understanding their rheological responses. Previously, it is important to highlight that the freezing process of the samples was conducted under a vacuum. The aim was to prevent the solidification of water from forming crystals that would damage the arrangement of microgels and nanosheets in the sample structure.

Initially, it is relevant to evaluate the microstructure of the hydrogels without the AFGO suspension to evaluate later the differences that the nanosheets cause in the microstructure of the hydrogels. The images of base hydrogels with pH 5, 7, and 9 are displayed in Figs. 7(a)–7(c).

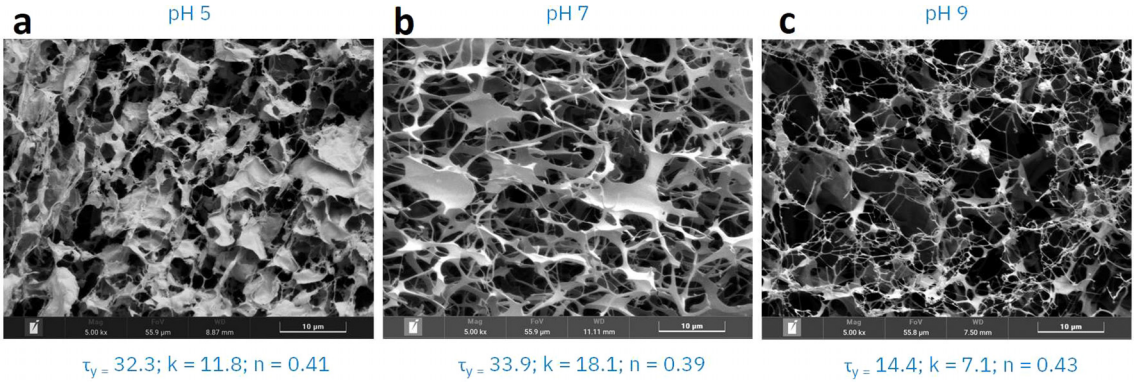

FIG. 7. Base hydrogel cryomicrographs. (a) Hydrogel at pH 5. (b) Hydrogel at pH 7. (c) Hydrogel at pH 9. The Herschel–Bulkley parameters associated with each microstructure have the following units: τ_y = Pa, k = Pa s^{-n}, and n = dimensionless.

02 February 2024 10:55:50

Published under an exclusive license by AIP Publishing

In general, it is possible to identify from the images that the solid content of hydrogels is structured in two formats: one that resembles a flatter structure, which will be called flakes, and a more linear one, which interconnects the flakes and which here will be called fibers. Such connections indicate the formation of a 3D structure responsible for the gel characteristic of the system.

It is worth pointing out that the samples did not show a honeycomb structure, usually associated with water crystallization. Also, the hydrogel structure, mainly at pH 7, is very similar to Carbopol confocal microscopy images presented in the literature.[78] These are indications that the sample freezing procedure was successful.

Upon comparing the images for the base hydrogels, it is evident that the pH 7 gel exhibits a more robust microstructure, boasting thicker flakes and fibers. This is consistent with the rheological results and the Carbopol zeta potential. Despite being well structured, the pH 5 hydrogel, with weaker and porous flakes, appears slightly more fragile. Following its rheological properties, the hydrogel with pH 9 has a more fragile structure, with fewer flakes and finer fibers. The effects of pH variation on the hydrogel microstructures are visible.

Before analyzing the visual effects of the AFGO on the suspension microstructure, it is necessary to understand how the nanosheets appear in the images. It is not easy to differentiate the nanosheets into the Carbopol 3D network structures.

Figure 8 shows that the AFGO identification in the suspension is only possible when the nanosheet is wholly exposed in the plane where the image was obtained. Thus, it is impossible to determine what the flake-like Carbopol structures or the AFGO nanosheets are.

Additionally, the increased concentration of nanosheets in the suspension enlarges the density of solids in the images. Therefore, the parameters to be considered in the analysis must be different. In this way, the characteristic to be evaluated will be the fiber profile of the suspensions.

Figure 9 shows the images obtained by cryomicroscopic analysis of the base hydrogels and suspensions with different concentrations of nanosheets prepared at pH 5, 7, and 9.

For the suspensions carried out at pH 5, the images show that the increase in the AFGO concentration weakens the hydrogel microstructure. The fibers that connect the flakes become increasingly thinner to the point of breaking, as it is possible to see in Fig. 9(c), which displays the cryomicrograph of the suspension with 5 mg/mL of AFGO. It is even noticeable that some flake structures are also weakened. The images also suggest that Carbopol microgels decrease in volume with increasing AFGO concentrations, which agrees with the Zeta potential results. This sample was the one that presented the lowest values of yield stress, viscosity, and elasticity. The polymer chain subjected to such conditions would be the most affected.

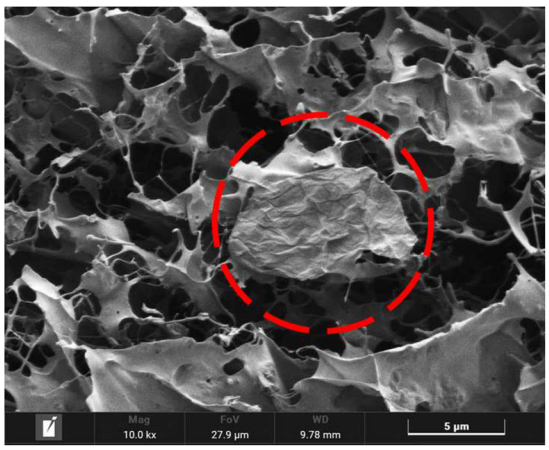

FIG. 8. Cryomicrographic image of an amino-functionalized graphene oxide (AFGO) nanosheet suspended in Carbopol hydrogel.

Just as noted for the samples prepared with pH 5, the increase in the concentration of nanosheets in the gels with pH 7 leads to the weakening of the suspension microstructure with a decrease in the thickness and eventual rupture of the fibers. Despite this behavior, the microstructures of suspensions at pH 7 are more robust than samples at pH 5. Such behavior is also consistent with the rheological results.

A discussion is necessary on reducing the fiber thickness of the hydrogel microstructures as nanosheet concentration increases. This behavior converges with the idea that the presence of nanosheets impairs the Carbopol swelling. For base hydrogels, mainly with pH 5 and 7, the microgels are pretty swollen and, therefore, have a considerable volume of water inside the macromolecule. Free water evaporates more efficiently during the sublimation process, while the water "trapped" within the macromolecules remains there. With an increase in the AFGO concentration, there is less water inside the macromolecule. Therefore, the fibers observed in the images become more fragile, as there was a larger amount of free water in the system, which evaporated. In the most critical cases, where there is a higher concentration of AFGO at pH 5 and 7, it is possible to note the contours of what would be the Carbopol macromolecules.

Figure 10 presents these cases with images obtained at higher magnifications. Figures 10(a) and 10(c) show images of the sample with pH 7 and 5 mg/mL of AFGO, while Figs. 10(b) and 10(d) present images of the suspension of 5 mg/mL of AFGO in hydrogel at pH 5.

With a less charged surface and lower osmosis, in addition to having a smaller volume, macromolecules also interact less with their surroundings. With sublimation, even more water evaporates, and in many areas of the samples, it is possible to see the outline of the polymer. In the suspension with 5 mg/mL of AFGO concentration in the hydrogel with pH 7, the polymer forms appear more smoothly on the surfaces of the fibers and flakes, which would be many nanometric spheres close to each other. On the other hand, for the sample with the highest AFGO concentration at pH 5, the deswelling of the macromolecules was quite abrupt, and the evaporation of water occurred practically entirely in some areas, which indicates a lack of interaction between the polymer and the solvent. Another discussion that can be associated with such images is related to the dimensions of Carbopol macromolecules. The images suggest the estimate that dry Carbopol particles are between 0.2 and 7 μm in size[67] contemplate indeed clusters of multi-macromolecules and not individual macromolecules.

Finally, for suspensions prepared at pH 9, it is notorious that the portion of solids increases in the images with the introduction of AFGO nanosheets. However, unlike what was observed for the samples at pH 5 and 7, the increase in the concentration of nanosheets does not affect the thickness of the fibers present in the microstructure so clearly. Therefore, it would not be possible to indicate, through the images, which sample has the most fragile microstructure.

02 February 2024 10:55:50

Published under an exclusive license by AIP Publishing

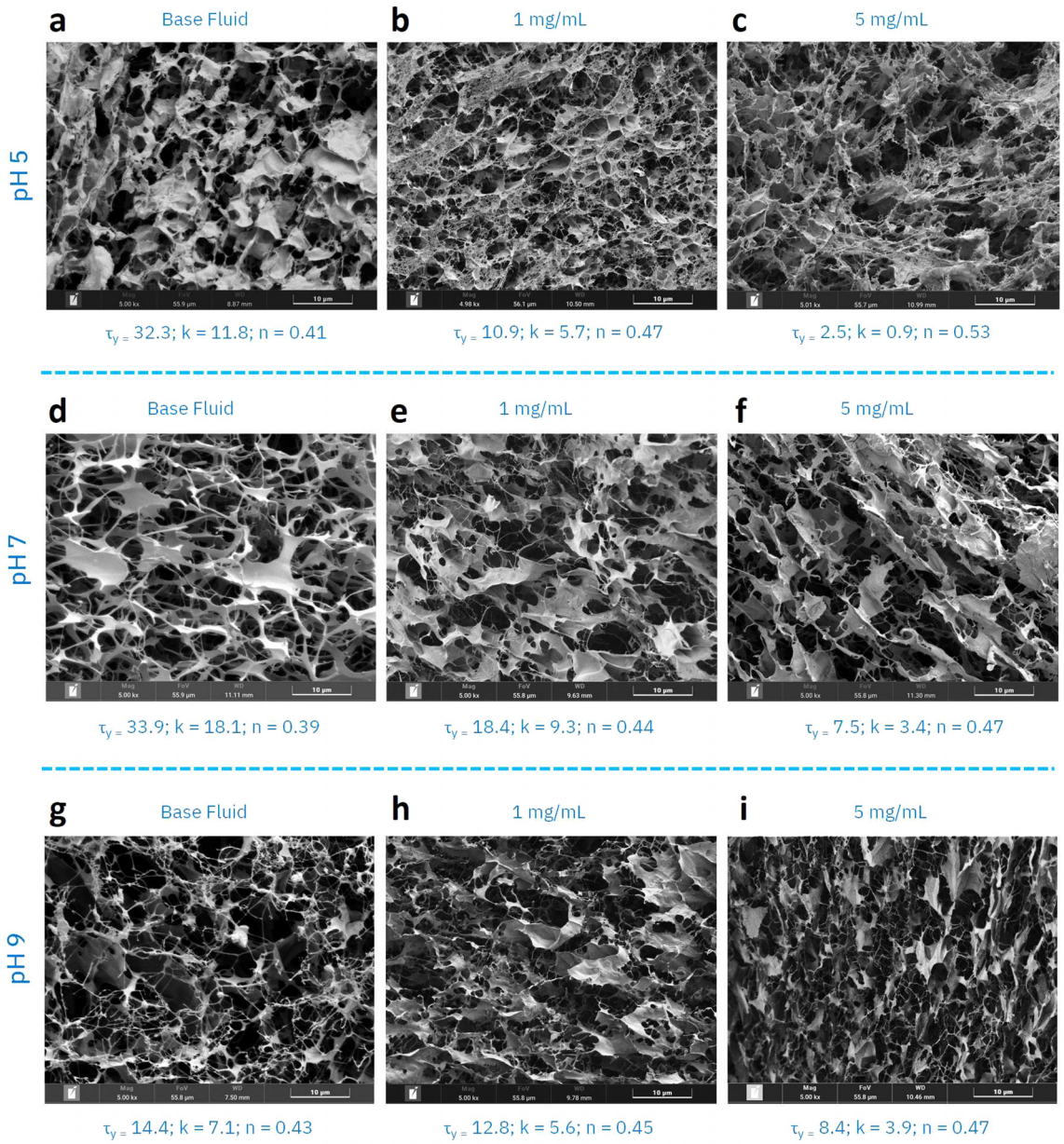

FIG. 9. Cryomicrographic images of the base hydrogels and suspensions with different AFGO concentrations. Each line in this figure concerns a pH. (a) Base hydrogel at pH 5. (b) 1 mg/mL AFGO suspension at pH 5. (c) 5 mg/mL AFGO suspension at pH 5. (d) Base hydrogel at pH 7. (e) 1 mg/mL AFGO suspension at pH 7. (f) 5 mg/mL AFGO suspension at pH 7. (g) Base hydrogel at pH 9. (h) 1 mg/mL AFGO suspension at pH 9. (i) 5 mg/mL AFGO suspension at pH 9. The Herschel–Bulkley parameters associated with each microstructure have the following units: $\tau_y = \text{Pa}$, $k = \text{Pa s}^{-n}$, and $n =$ dimensionless.

This behavior also agrees with the rheological results. Samples prepared at pH 9 showed the lowest rheological variation with increasing AFGO concentration.

The results have shown the effects of AFGO concentration and pH media on the microstructure and rheological behavior of AFGO suspensions in Carbopol hydrogels. The data obtained demonstrate that the various techniques used converge and describe the behavior of suspensions, pointing out causes and indicating their effects.

IV. FINAL REMARKS

This study showed the effects of amino-functionalized graphene oxide (AFGO) concentration and pH media on the microstructure and rheological behavior of AFGO suspensions in Carbopol hydrogels. The obtained data demonstrates the convergence of various techniques for describing and explaining the behavior of suspensions, including their causes and effects. Hydrogels find application across multiple

02 February 2024 10:55:50

Published under an exclusive license by AIP Publishing

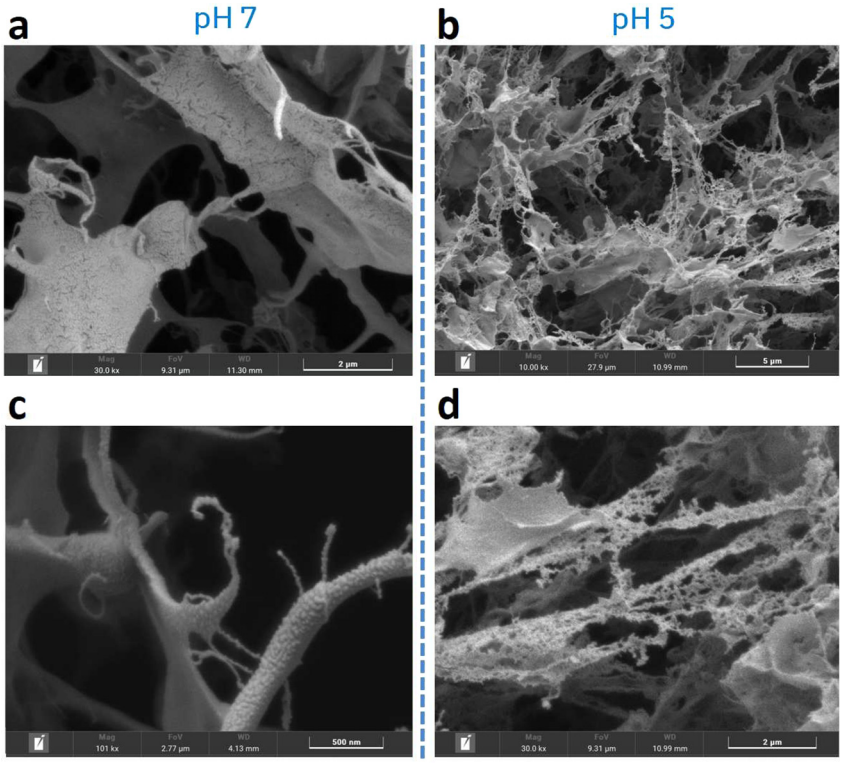

FIG. 10. Effect of higher AFGO concentrations on the Carbopol microgel swelling and the consequent microstructure of suspensions prepared at lower pHs. (a) Cryomicrograph of the 5 mg/mL AFGO suspension at pH 7 with 30.000× magnification. (b) Cryomicrograph of the 5 mg/mL AFGO suspension at pH 5 with 10.000× magnification. (c) Cryomicrograph of the 5 mg/mL AFGO suspension at pH 7 with 100.000× magnification. (d) Cryomicrograph of the 5 mg/mL AFGO suspension at pH 5 with 30.000× magnification.

industries, and the incorporation of nanoparticles can enhance their functionality and expand their range of uses. To optimize the flow of such nanofluids in industrial processes, it is crucial to understand the rheology of the final nanofluid.

Through physicochemical characterization, it was possible to confirm that the modified Hummers method successfully oxidized the graphite. Moreover, the microwave-assisted functionalization of graphene oxide with triethylenetetramine (TETA) allowed for the covalent attachment of amine groups to the graphene oxide nanosheets.

All analyzed systems presented yield stress and shear thinning behavior, and the viscosity is well modeled by the Herschel–Bulkley equation. The viscoelastic characteristics were also investigated. All samples showed a storage modulus larger than the viscous modulus in the linear viscoelastic region.

The system electrostatic balance proved decisive for the microstructure and rheological behavior of hydrogels and suspensions. The pH of the medium had a direct effect on the degree of ionization of Carbopol macromolecules. Elevating pH leads to increased ionization of polymer chains and consequently increases the volume of microgels. However, as the pH rises, the concentration of counterions in the microgels' surroundings also increases. From a certain point onwards, the high concentration of counterions in the solvent starts to impair the volumetric expansion of the polymer. As a result, as the pH increases and the polymer expands, the viscosity tends to enhance. This occurs until the concentration of counterions in the system starts to act by reducing the volume of the microgels, consequently reducing the hydrogel viscosity.

AFGO nanosheets influence the electrostatic balance of the system. At all pHs, the increase in nanosheet concentration led to a decrease in rheological characteristics (viscosity, yield stress, storage, and loss moduli). AFGO starts to compete with Carbopol in the deprotonation of carboxylic acids. As they have a lower pKa value, the nanosheets deprotonate more quickly, reducing the deprotonation capacity of the microgels. Consequently, the macromolecules decrease in volume, leading to the gel's weakening and a consequent drop in viscosity, yield stress, and elastic and viscous moduli. The zeta potential results indicated that this phenomenon is even more pronounced at lower pHs. At pH 9, the greatest influence of the nanosheets suspension is the lower interaction strength between AFGO and Carbopol, which decreases the hydrogel's viscosity.

These effects were visible through scanning electron cryomicroscopic analysis of the samples. The images indicate a reduction in the volume of the microgels with an increase in the concentration of nanosheets, and it is even possible to visualize the contours of the polymer chains in suspensions with a higher AFGO concentration and lower pH.

The results indicate that the union of these two polyelectrolytes in a system can still provide a gel, even with a more fragile microstructure than those obtained with the dispersion of Carbopol alone. Depending on the application, it will be necessary to use higher concentrations of the polymer to obtain the necessary rheology. However, it is worth highlighting that these results are associated with the specific characteristics of the nanosheets used. The number of amino groups attached to the nanosheets was insufficient to modify the sign of the net surface charge since the zeta potential of AFGO in all pH ranges was negative. Thus, the higher amount of carboxylic groups present in the nanosheets was predominant in the rheological behavior of the suspensions. Therefore, the use of modified GO nanosheets with

02 February 2024 10:55:50

Published under an exclusive license by AIP Publishing

positive surface charge or functional chemical groups that do not directly compete with Carbopol carboxylic acids can lead to more favorable rheological point of view. This subject should be further explored.

SUPPLEMENTARY MATERIAL

See the supplementary material for detailed information on the preparation of AFGO and suspensions. The material also reports the methodologies used to characterize nanosheets, as well as the results and discussions of the physical and chemical properties obtained.

ACKNOWLEDGMENTS

This research was supported by FAPERJ. Thanks to the support of the National Petroleum Agency (ANP) and the Studies and Projects Financier (Finep). Many thanks to Dr. Priscilla Varges for her help and useful discussions during the rheological experiments. Finally, Dr. Eliana Marin is thanked for her help and useful discussions on cryo-SEM experiments.

AUTHOR DECLARATIONS

Conflict of Interest

The authors have no conflicts to disclose.

Author Contributions

Lorena Rodrigues da Costa Moraes: Conceptualization (equal); Data curation (equal); Formal analysis (equal); Investigation (equal); Methodology (equal); Validation (equal); Visualization (equal); Writing – original draft (equal); Writing – review & editing (equal). **Helio Ribeiro:** Conceptualization (equal); Data curation (equal); Investigation (equal); Methodology (equal); Resources (equal); Supervision (equal); Validation (equal); Visualization (equal); Writing – original draft (equal); Writing – review & editing (equal). **Ricardo J. E. Andrade:** Conceptualization (equal); Formal analysis (equal); Funding acquisition (equal); Investigation (equal); Methodology (equal); Project administration (equal); Resources (equal); Supervision (equal); Writing – review & editing (equal). **Mônica Feijó Naccache:** Conceptualization (equal); Formal analysis (equal); Funding acquisition (equal); Methodology (equal); Project administration (equal); Supervision (equal); Writing – review & editing (equal).

DATA AVAILABILITY

The data that support the findings of this study are available from the corresponding author upon reasonable request.

REFERENCES

[1]V. Georgakilas, M. Otyepka, A. B. Bourlinos, V. Chandra, N. Kim, K. C. Kemp, P. Hobza, R. Zboril, and K. S. Kim, "Functionalization of graphene: Covalent and non-covalent approaches, derivatives and applications," Chem. Rev. **112**, 6156–6214 (2012).

[2]A. Khan, M. Jawaid, B. Neppolian, and A. M. Asiri, *Graphene Functionalization Strategies* (Springer, 2019).

[3]M. Song and D. Cai, "Graphene functionalization: A review," Polym.-Graphene Nanocompos. **26**, 1–51 (2012).

[4]G.-H. Yang, D.-D. Bao, H. Liu, D.-Q. Zhang, N. Wang, and H.-T. Li, "Functionalization of graphene and applications of the derivatives," J. Inorg. Organomet. Polym. **27**, 1129–1141 (2017).

[5]T. Kuila, S. Bose, A. K. Mishra, P. Khanra, N. H. Kim, and J. H. Lee, "Chemical functionalization of graphene and its applications," Prog. Mater. Sci. **57**, 1061–1105 (2012).

[6]S. Liu, A. K. Bastola, and L. Li, "A 3D printable and mechanically robust hydrogel based on alginate and graphene oxide," ACS Appl. Mater. Interfaces **9**, 41473–41481 (2017).

[7]S. Ling, W. Kang, S. Tao, and C. Zhang, "Highly concentrated graphene oxide ink for facile 3D printing of supercapacitors," Nano Mater. Sci. **1**, 142–148 (2019).

[8]K. Fu, Y. Wang, C. Yan, Y. Yao, Y. Chen, J. Dai, S. Lacey, Y. Wang, J. Wan, T. Li *et al.*, "Graphene oxide-based electrode inks for 3D-printed lithium-ion batteries," Adv. Mater. **28**, 2587–2594 (2016).

[9]E. Garcia-Tunon, E. Feilden, H. Zheng, E. D'Elia, A. Leong, and E. Saiz, "Graphene oxide: An all-in-one processing additive for 3D printing," ACS Appl. Mater. Interfaces **9**, 32977–32989 (2017).

[10]J. Zhong, G.-X. Zhou, P.-G. He, Z.-H. Yang, and D.-C. Jia, "3D printing strong and conductive geo-polymer nanocomposite structures modified by graphene oxide," Carbon **117**, 421–426 (2017).

[11]D. V. Kosynkin, G. Ceriotti, K. C. Wilson, J. R. Lomeda, J. T. Scorsone, A. D. Patel, J. E. Friedheim, and J. M. Tour, "Graphene oxide as a high-performance fluid-loss-control additive in water-based drilling fluids," ACS Appl. Mater. Interfaces **4**, 222–227 (2012).

[12]S. Liu, Z. Chen, Q. Meng, H. Zhou, C. Li, and B. Liu, "Effect of graphene and graphene oxide addition on lubricating and friction properties of drilling fluids," Nanosci. Nanotechnol. Lett. **9**, 446–452 (2017).

[13]T. A. Saleh, A. Rana, and M. K. Arfaj, "Graphene grafted with polyethyleneimine for enhanced shale inhibition in the water-based drilling fluid," Environ. Nanotechnol., Monit. Manage. **14**, 100348 (2020).

[14]L. Lei, Z. Xia, L. Zhang, Y. Zhang, and L. Zhong, "Preparation and properties of amino-functional reduced graphene oxide/waterborne polyurethane hybrid emulsions," Prog. Org. Coat. **97**, 19–27 (2016).

[15]P. Haghdadeh, M. Ghaffari, B. Ramezanzadeh, G. Bahlakeh, and M. R. Saeb, "The role of functionalized graphene oxide on the mechanical and anti-corrosion properties of polyurethane coating," J. Taiwan Inst. Chem. Eng. **86**, 199–212 (2018).

[16]S. Pourhashem, A. Rashidi, M. R. Vaezi, and M. R. Bagherzadeh, "Excellent corrosion protection performance of epoxy composite coatings filled with amino-silane functionalized graphene oxide," Surf. Coat. Technol. **317**, 1–9 (2017).

[17]T. Sun, H. Zou, Y. Zhou, R. Li, M. Liang, and Y. Chen, "Achieving high-performance epoxy nanocomposites with trifunctional poly (oxypropylene) amines functionalized graphene oxide," High Perform. Polym. **31**, 557–569 (2019).

[18]S. Wang, J. Wang, W. Zhang, J. Ji, Y. Li, G. Zhang, F. Zhang, and X. Fan, "Ethylenediamine modified graphene and its chemically responsive supramolecular hydrogels," Ind. Eng. Chem. Res. **53**, 13205–13209 (2014).

[19]S. H. Ryu, J. Sin, and A. Shanmugharaj, "Study on the effect of hexamethylene diamine functionalized graphene oxide on the curing kinetics of epoxy nanocomposites," Eur. Polym. J. **52**, 88–97 (2014).

[20]T. Missala, R. Szewczyk, W. Winiarski, M. Hamela, M. Kamiński, S. Dąbrowski, D. Pogorzelski, M. Jakubowska, and J. Tomasik, "Study on tribological properties of lubricating grease with additive of graphene," in *Progress in Automation, Robotics and Measuring Techniques* (Springer, 2015), pp. 181–187.

[21]X. Fan, Y. Xia, L. Wang, and W. Li, "Multilayer graphene as a lubricating additive in bentone grease," Tribol. Lett. **55**, 455–464 (2014).

[22]Z.-L. Cheng and X.-X. Qin, "Study on friction performance of graphene-based semi-solid grease," Chin. Chem. Lett. **25**, 1305–1307 (2014).

[23]H. Kinoshita, Y. Nishina, A. A. Alias, and M. Fujii, "Tribological properties of monolayer graphene oxide sheets as water-based lubricant additives," Carbon **66**, 720–723 (2014).

[24]S. S. Rawat, A. Harsha, A. Chouhan, and O. Khatri, "Effect of graphene-based nanoadditives on the tribological and rheological performance of paraffin grease," J. Mater. Eng. Perform. **29**, 2235–2247 (2020).

[25]S. Yi, G. Li, S. Ding, and J. Mo, "Performance and mechanisms of graphene oxide suspended cutting fluid in the drilling of titanium alloy Ti-6Al-4V," J. Manuf. Processes **29**, 182–193 (2017).

02 February 2024 10:55:50

Published under an exclusive license by AIP Publishing

[26]Q. Li, F. Li, X. Qi, F. Wei, H. Chen, and T. Wang, "Pluronic® f127 stabilized reduced graphene oxide hydrogel for the treatment of psoriasis: *In vitro* and *in vivo* studies," Colloids Surf., B **195**, 111246 (2020).
[27]H. Li, Y. Jia, and C. Liu, "Pluronic® f127 stabilized reduced graphene oxide hydrogel for transdermal delivery of ondansetron: Ex vivo and animal studies," Colloids Surf., B **195**, 111259 (2020).
[28]N. D. Bikiaris, I. Koumentakou, S. Lykidou, and N. Nikolaidis, "Innovative skin product o/w emulsions containing lignin, multiwall carbon nanotubes and graphene oxide nanoadditives with enhanced sun protection factor and uv stability properties," Appl. Nano **3**, 1–15 (2022).
[29]W. Shao, C. Liu, H. Ma, Z. Hong, Q. Xie, and Y. Lu, "Fabrication of pH-sensitive thin-film nanocomposite nanofiltration membranes with enhanced performance by incorporating amine-functionalized graphene oxide," Appl. Surf. Sci. **487**, 1209–1221 (2019).
[30]J. Lee, H.-R. Chae, Y. J. Won, K. Lee, C.-H. Lee, H. H. Lee, I.-C. Kim, and J-m Lee, "Graphene oxide nanoplatelets composite membrane with hydrophilic and antifouling properties for wastewater treatment," J. Membr. Sci. **448**, 223–230 (2013).
[31]C. Zhao, X. Xu, J. Chen, G. Wang, and F. Yang, "Highly effective antifouling performance of PVDF/graphene oxide composite membrane in membrane bioreactor (MBR) system," Desalination **340**, 59–66 (2014).
[32]M. Wang, H. Yao, R. Wang, and S. Zheng, "Chemically functionalized graphene oxide as the additive for cement–matrix composite with enhanced fluidity and toughness," Constr. Build. Mater. **150**, 150–156 (2017).
[33]M. Hu, J. Guo, J. Fan, D. Chen *et al.*, "Dispersion of triethanolamine-functionalized graphene oxide (tea-go) in pore solution and its influence on hydration, mechanical behavior of cement composite," Constr. Build. Mater. **216**, 128–136 (2019).
[34]Y. Shang, D. Zhang, C. Yang, Y. Liu, and Y. Liu, "Effect of graphene oxide on the rheological properties of cement pastes," Constr. Build. Mater. **96**, 20–28 (2015).
[35]L. R. da C. Moraes, H. Ribeiro, E. Cargnin, R. J. E. Andrade, and M. F. Naccache, "Rheology of graphene oxide suspended in yield stress fluid," J. Non-Newtonian Fluid Mech. **286**, 104426 (2020).
[36]P. Paraskar, P. Bari, and S. Mishra, "Influence of amine functionalized graphene oxide on mechanical and thermal properties of epoxy matrix composites," Iran. Polym. J. **29**, 47–55 (2020).
[37]J. Jang, I. Park, S.-S. Chee, J.-H. Song, Y. Kang, C. Lee, W. Lee, M.-H. Ham, and I. S. Kim, "Graphene oxide nanocomposite membrane cooperatively cross-linked by monomer and polymer overcoming the trade-off between flux and rejection in forward osmosis," J. Membr. Sci. **598**, 117684 (2020).
[38]W. Zhang, J. Ma, D. Gao, Y. Zhou, C. Li, J. Zha, and J. Zhang, "Preparation of amino-functionalized graphene oxide by Hoffman rearrangement and its performances on polyacrylate coating latex," Prog. Org. Coat. **94**, 9–17 (2016).
[39]F. Ferreira, F. Brito, W. Franceschi, E. Simonetti, L. Cividanes, M. Chipara, and K. Lozano, "Functionalized graphene oxide as reinforcement in epoxy based nanocomposites," Surf. Interfaces **10**, 100–109 (2018).
[40]L. Mei, C. Lin, F. Cao, D. Yang, X. Jia, S. Hu, X. Miao, and P. Wu, "Amino-functionalized graphene oxide for the capture and photothermal inhibition of bacteria," ACS Appl. Nano Mater. **2**, 2902–2908 (2019).
[41]B.-Y. Lu, G.-Y. Zhu, C.-H. Yu, G.-Y. Chen, C.-L. Zhang, X. Zeng, Q.-M. Chen, and Q. Peng, "Functionalized graphene oxide nanosheets with unique three-in-one properties for efficient and tunable antibacterial applications," Nano Res. **14**, 185–190 (2021).
[42]S. Curran, R. Hayes, A. Afacan, M. Williams, and P. Tanguy, "Properties of Carbopol solutions as models for yield-stress fluids," J. Food Sci. **67**, 176–180 (2002).
[43]A. A. Balandin, S. Ghosh, W. Bao, I. Calizo, D. Teweldebrhan, F. Miao, and C. N. Lau, "Superior thermal conductivity of single-layer graphene," Nano Lett. **8**, 902–907 (2008).
[44]D. C. Marcano, D. V. Kosynkin, J. M. Berlin, A. Sinitskii, Z. Sun, A. Slesarev, L. B. Alemany, W. Lu, and J. M. Tour, "Improved synthesis of graphene oxide," ACS Nano **4**, 4806–4814 (2010).
[45]H. Ribeiro, W. M. da Silva, J. C. Neves, H. D. R. Calado, R. Paniago, L. M. Seara, D. das Mercês Camarano, and G. G. Silva, "Multifunctional nanocomposites based on tetraethylenepentamine-modified graphene oxide/epoxy," Polym. Test. **43**, 182–192 (2015).
[46]D. Q. Craig, S. Tamburic, G. Buckton, and J. M. Newton, "An investigation into the structure and properties of Carbopol 934 gels using dielectric spectroscopy and oscillatory rheometry," J. Controlled Release **30**, 213–223 (1994).
[47]B. Barry and M. Meyer, "The rheological properties of Carbopol gels. I. Continuous shear and creep properties of Carbopol gels," Int. J. Pharm. **2**, 1–25 (1979).
[48]"Carbopol® polymer products," https://www.lubrizol.com/Health/Pharmaceuticals/Excipients/Carbopol-Polymer-Products (accessed 08-16-2022).
[49]P. Coussot, F. Bertrand, and B. Herzhaft, "Rheological behavior of drilling muds, characterization using MRI visualization," Oil Gas Sci. Technol. **59**, 23–29 (2004).
[50]P. R. Varges, C. M. Costa, B. S. Fonseca, M. F. Naccache, and P. R. de Souza Mendes, "Rheological characterization of Carbopol® dispersions in water and in water/glycerol solutions," Fluids **4**, 3 (2019).
[51]F. K. Oppong, L. Rubatat, B. J. Frisken, A. E. Bailey, and J. R. De Bruyn, "Microrheology and structure of a yield-stress polymer gel," Phys. Rev. E **73**, 041405 (2006).
[52]Lubrizol Advanced Materials Inc., "Neutralizing Carbopol™ and pemulen™ polymers in aqueous and hydroalcoholic systems," Technical Data Sheet TDS-237 (2009).
[53]R. Ketz, R. Prud'homme, and W. Graessley, "Rheology of concentrated microgel solutions," Rheol. Acta **27**, 531–539 (1988).
[54]I. A. Gutowski, D. Lee, J. R. de Bruyn, and B. J. Frisken, "Scaling and mesostructure of Carbopol dispersions," Rheol. Acta **51**, 441–450 (2012).
[55]J.-Y. Kim, J.-Y. Song, E.-J. Lee, and S.-K. Park, "Rheological properties and microstructures of Carbopol gel network system," Colloid Polym. Sci. **281**, 614–623 (2003).
[56]M. T. Islam, N. Rodriguez-Hornedo, S. Ciotti, and C. Ackermann, "Rheological characterization of topical carbomer gels neutralized to different pH," Pharm. Res. **21**, 1192–1199 (2004).
[57]J.-M. Piau, "Carbopol gels: Elastoviscoplastic and slippery glasses made of individual swollen sponges: Meso-and macroscopic properties, constitutive equations and scaling laws," J. Non-Newtonian Fluid Mech. **144**, 1–29 (2007).
[58]F. Renou, J. Stellbrink, and G. Petekidis, "Yielding processes in a colloidal glass of soft star-like micelles under large amplitude oscillatory shear (LAOS)," J. Rheol. **54**, 1219–1242 (2010).
[59]C. Perge, N. Taberlet, T. Gibaud, and S. Manneville, "Time dependence in large amplitude oscillatory shear: A rheo-ultrasonic study of fatigue dynamics in a colloidal gel," J. Rheol. **58**, 1331–1357 (2014).
[60]C. Kugge, N. Vanderhoek, and D. Bousfield, "Oscillatory shear response of moisture barrier coatings containing clay of different shape factor," J. Colloid Interface Sci. **358**, 25–31 (2011).
[61]M. Dinkgreve, J. Paredes, M. M. Denn, and D. Bonn, "On different ways of measuring "the" yield stress," J. Non-Newtonian Fluid Mech. **238**, 233–241 (2016).
[62]W. Y. Shih, W.-H. Shih, and I. A. Aksay, "Elastic and yield behavior of strongly flocculated colloids," J. Am. Ceram. Soc. **82**, 616–624 (1999).
[63]J. E. Elliott, M. Macdonald, J. Nie, and C. N. Bowman, "Structure and swelling of poly (acrylic acid) hydrogels: Effect of pH, ionic strength, and dilution on the crosslinked polymer structure," Polymer **45**, 1503–1510 (2004).
[64]P. Coussot, L. Tocquer, C. Lanos, and G. Ovarlez, "Macroscopic vs. local rheology of yield stress fluids," J. Non-Newtonian Fluid Mech. **158**, 85–90 (2009).
[65]F. Oppong and J. De Bruyn, "Mircorheology and jamming in a yield-stress fluid," Rheol. Acta **50**, 317–326 (2011).
[66]E. Di Giuseppe, F. Corbi, F. Funiciello, A. Massmeyer, T. Santimano, M. Rosenau, and A. Davaille, "Characterization of Carbopol[textregistered] hydrogel rheology for experimental® tectonics and geodynamics," Tectonophysics **642**, 29–45 (2015).
[67]See https://www.lubrizol.com/-/media/Lubrizol/Health/TDS/TDS-222_Molecular_Weight_Carbopol_-Polymers.pdf for "lubrizol.com" (last accessed October 27, 2023).
[68]K. G. Wilcox, S. K. Kozawa, and S. Morozova, "Fundamentals and mechanics of polyelectrolyte gels: Thermodynamics, swelling, scattering, and elasticity," Chem. Phys. Rev. **2**, 041309 (2021).

02 February 2024 10:55:50

Published under an exclusive license by AIP Publishing

[69]M. Ullner, K. Qamhieh, and B. Cabane, "Osmotic pressure in polyelectrolyte solutions: Cell-model and bulk simulations," Soft matter **14**, 5832–5846 (2018).
[70]M. Toepke and W. Murphy, "1.31 dynamic hydrogels," Compr. Biomater. **1**, 705 (2017).
[71]A. V. Dobrynin, "Polyelectrolytes: On the doorsteps of the second century," Polymer **202**, 122714 (2020).
[72]S. R. Raghavan, L. A. Chen, C. McDowell, S. A. Khan, R. Hwang, and S. White, "Rheological study of crosslinking and gelation in chlorobutyl elastomer systems," Polymer **37**, 5869–5875 (1996).
[73]J. Mewis and N. J. Wagner, "Thixotropy," Adv. Colloid Interface Sci. **147–148**, 214–227 (2009).
[74]A. Puisto, M. Mohtaschemi, M. J. Alava, and X. Illa, "Dynamic hysteresis in the rheology of complex fluids," Phys. Rev. E **91**, 042314 (2015).
[75]C. N. Lunardi, A. J. Gomes, F. S. Rocha, J. De Tommaso, and G. S. Patience, "Experimental methods in chemical engineering: Zeta potential," Can. J. Chem. Eng. **99**, 627–639 (2021).
[76]L. Nová, F. Uhlík, and P. Košovan, "Local pH and effective pKa of weak polyelectrolytes–insights from computer simulations," Phys. Chem. Chem. Phys. **19**, 14376–14387 (2017).
[77]J. Landsgesell, L. Nová, O. Rud, F. Uhlík, D. Sean, P. Hebbeker, C. Holm, and P. Košovan, "Simulations of ionization equilibria in weak polyelectrolyte solutions and gels," Soft Matter **15**, 1155–1185 (2019).
[78]P. Lefrançois, E. Ibarboure, B. Payré, E. Gontier, J.-F. Le Meins, and C. Schatz, "Insights into Carbopol gel formulations: Microscopy analysis of the microstructure and the influence of polyol additives," J. Appl. Polym. Sci. **132**, 42761 (2015).

02 February 2024 10:55:50

Published under an exclusive license by AIP Publishing